Archives of Environmental Protection
Vol. 46 no. 1 pp. 62–75

PL ISSN 2083-4772
DOI 10.24425/aep.2020.132527

Multi-component sorption and utilization of solid waste to simultaneous removing basic dye and heavy metal from aqueous system

Eleonora Sočo*, Dariusz Pająk, Jan Kalembkiewicz

Department of Inorganic and Analytical Chemistry, University of Technology, Rzeszów, Poland

*Corresponding author's e-mail: eleonora@prz.edu.pl

Keywords: heavy metal, immobilization, sorption, waste material, bi-component system, basic dye.

Abstract: The presented work introduces a simple modification of coal fly ash (FA) with 30% solution of H_2O_2, used as a new efficient sorbent for the removal of organic dye crystal violet (CV) in the presence of Cu(II) ions in single- and bi-component systems Cu(II)-CV. FT-IR, TG, SEM-EDS, and XRD suggested that the mechanism of Cu(II) and CV sorption onto FA-H_2O_2 includes ion-exchange and surface adsorption process. Comparing the values of the reduced chi-square test (χ^2/DoF) and the determination coefficient R^2 obtained for CV of the considered isotherms, the fitting degree follows the sequence: Jovanović > Langmuir > Elovich > Freundlich > Redlich-Peterson (R-P) > Tóth > Halsey > BET. Sorption of Cu(II) ions in a single system by means of FA-H_2O_2 was well fitted by the Langmuir and R-P model. The studies of equilibrium in a bi-component system by means of extended Langmuir (EL), extended Langmuir-Freundlich (ELF), and Jain-Snoeyink (JS) models were analysed. The estimation of parameters of sorption isotherms in a bi-component system Cu(II)-CV has shown that the best of fit calculated values of experimental data for both sorbates have been the EL model and the JS model, but only in the case of a CV dye. The sorption kinetic of Cu(II) and CV onto FA-H_2O_2 was discussed by means of the PFO, PSO, and intra-particle diffusion models.

Abbreviations

a_{RP} – Redlich and Peterson constant, $(L \cdot mg^{-1})^B$
B – Redlich and Peterson heterogeneity factor
bi – boundary layer thickness, $mg \cdot g^{-1}$
C_0 – initial concentration of Cd(II) and CV, $mg \cdot L^{-1}$
C_e – concentration of Cd(II) and CV in solution at the sorption equilibrium, $mg \cdot L^{-1}$
CV – crystal violet
DoF – degrees of freedom
DTA – differential thermal analysis
DTG – differential thermogravimetric analysis
FA – fly ash
FAAS – Flame Atomic Absorption Spectrometry
FA-H_2O_2 – H_2O_2 treated fly ash
FT-IR – Fourier transform infrared spectroscopy
K_{BET} – Brunauer, Emmett and Teller sorption coefficient
K_E – Elovich sorption coefficient, $L \cdot mg^{-1}$
K_F – Freundlich sorption coefficient, $mg^{1-1/n} \cdot L^{1/n} \cdot g^{-1}$
K_H – Halsey sorption coefficient, $mg^{n+1} \cdot g^{-1} \cdot L^{-1}$
K_J – Jovanović sorption coefficient, $L \cdot mg^{-1}$
K_L – Langmuir sorption coefficient, $L \cdot mg^{-1}$
K_{RP} – Redlich and Peterson sorption coefficient, $L \cdot g^{-1}$
K_{Th} – Tóth sorption coefficient, $(L \cdot mg^{-1})^{Th}$
k_2 – constant of second order rate, $g \cdot mg^{-1} \cdot min^{-1}$
k_i' – constant of intra-particle diffusion rate, $mg \cdot g^{-1} \cdot min^{-1/2}$
n_F – Freundlich heterogeneity factor
n_H – Halsey heterogeneity factor
PFO – pseudo-first-order model
PSO – pseudo-second-order model
q_e – amount of Cd(II) and CV in sorbent at equilibrium (equilibrium sorption capacity), $mg \cdot g^{-1}$
q_{max} – maximum content of Cd(II) and CV in sorbent at the sorption equilibrium, $mg \cdot g^{-1}$
q_t – amount of Cd(II) and CV adsorbed on sorbent at time t, $mg \cdot g^{-1}$
q_0 – initial amount of Cd(II) and CV in the solution, $mg \cdot g^{-1}$
R^2 – linear regression coefficient
SEM-EDS – scanning electron microscope employing the detector of energy dispersive x-ray spectroscopy
t – time of sorption, min or h
TG – thermogravimetry
Th – Tóth heterogeneity factor
u – initial sorption rate, $mg \cdot g^{-1} \cdot min^{-1}$
XRD – x-ray diffraction
χ^2/DoF – reduced chi-square test

Introduction

Fly ash as a by-product derived from coal combustion in thermal power plant is gradually increasing amounts to approximately 500 million tons per year around the world (Ruhl et al. 2010). The amounts of fly ash generated annually are: 60 million tons for the USA, 38.5 million tons for Europe, and 700 million tons for China (Ahmaruzzaman 2010; Dai et al. 2012). Although its use in the building industry contributes to the reduction of environment problems: about 48% for Europe, 25–30% for the USA, and 40% for China (Canpolat et al. 2004; Dai et al. 2012) there is continuous interest in its recycling, by converting it into products for use in environmental applications (Ahmaruzzaman 2010).

In Poland, the coal plants produce about 4 million ton of ash per year. It is estimated that about 50% is recycled (statistical yearbook of Polish Central Statistical Office, 2018) and utilized in building materials mainly as an additive in cement, concrete, and structural filling. However, there is a proportion which is disposed in settling ponds, landfills or used to cover wells and exhausted mines. Differentiated physicochemical and mineralogical characteristics of fly ash are relevant for its potential application. For that reason, studies on utilization of this low cost adsorbent, which is suitable for the removal of heavy metals, dyes and organics from wastewaters, have gained much attention in recent years (Polowczyk et al. 2013). Hence, there have been studies performed on utilization of this low cost adsorbent for the removal of heavy metals and dyes from wastewaters. The study analyses physical and chemical changes of Polish coal fly ash from Rzeszów-Załęże heat-power station (Sočo and Kalembkiewicz 2015), with an oxidizing chemical agent and their abilities to remove heavy metals and organic dye from aqueous solutions in single and bi-component systems.

Adsorption is an attractive and effective process of the removal of heavy metals and dyes from wastewater, especially if the adsorbent is cheap and readily available. The chemical composition of fly ash, with abundance of amorphous aluminosilicate glass, which is the prevalent reactive phase, is what makes fly ash an important source material in low-cost sorbent synthesis (Gupta and Suhas 2009). What is more, a three-dimensional open structure makes hydrated aluminosilicate minerals extremely useful in solving the mobility of toxic elements in a number of environmental applications (Jiao et al. 2011). Therefore, coal fly ash and its converted fly ash may be the materials considered in the removal of heavy metals and dyes.

Another serious environmental problem is highly coloured wastewater which contains hazardous dyes. Dyes can be classified as anionic (direct, acid, and reactive dyes), cationic (basic dyes) or non-ionic (disperse dyes) (Alver and Metin 2012; Sarma et al. 2016).

The use of synthetic dyes is increasingly common in textile industries, dye manufacturing industries, paper and pulp mills, tanneries, electroplating factories, food companies, and others. In general, dyes are resistant to the following agents: light, heat and oxidization, and are usually non-biodegradable. In traditional biological and physical treatment most dyes are considered non-oxidizable substances (Anirudhan and Ramachandran 2015). Therefore, it is necessary to study the adsorption phenomena of the other class of dyes. Crystal violet (CV) is a basic dye which belongs to the group of tri-phenylmethanes (Amodu et al. 2015; Sarma et al. 2016). It is a typical cationic dye that has been widely used as a colorant in textile products. Incrustation is the most visible effect of wastewater discharge from the textile industry. What is more, incrustation reduces light penetration into the water and can adversely affect marine life (Amodu et al. 2015).

Copper is the most toxic, non-essential heavy metal present in the environment. Copper poisoning of humans causes nose, mouth and eyes irritation, induces headaches, stomachaches, and is responsible for dizziness, vomiting and diarrhea. Constantly recurring exposure to elevated levels of copper may lead to Wilson's disease, which is characterized by hepatic cirrhosis, brain damage, demyelization, renal disease, and copper deposition in the cornea (Luo et al. 2011).

In recent years, several studies on heavy metals and dyes immobilization by fly ash have been done. However, more information is still required to gain better understanding of the relationship between heavy metals and dyes sorption properties of fly ashes and their chemical composition (An and Huang 2012).

The presented study investigates the physical and chemical changes of Polish coal fly ash after chemical treatment with the hydrogen peroxide and its abilities to remove copper(II) and crystal violet from aqueous solutions in single and bi-component systems Cu(II)-CV.

Experimental analysis

Materials and methods

The coal fly ash sample was collected from the Rzeszów-Załęże (Poland) electric power station. The ash was derived from the combustion of bituminous coal. Fluidised bed combustion and dry sorbent injection systems for desulfurization were used. The various kinds and properties of fly ash were described by Franus et al. 2015. On the basis of the combined content over 70% of SiO_2, Al_2O_3 and Fe_2O_3 the coal fly ash defines as Class F defines according to the America Society for Testing Materials (ASTM C618) classification. The mean particle size distribution from the optic analyser is shown in Fig. 1. Particle size analysis was shown for volume median diameter (d50) of about 33.3 μm, while (d10) and (d90) were 3.7 and 91.6 μm, respectively. The plot of pore size distribution indicated that the majority of particles have a span of 2.6 ((d90-d10)/d50). The values of BET surface area (111.3 $m^2 \cdot g^{-1}$), pore size (5.87 nm) and pore volume (0.171 $cm^3 \cdot g^{-1}$) were measured. The N_2 adsorption/desorption hysteresis loop suggested the presence of mesopores (2–50 nm) between the slits of the micropores (below 2 nm) and the possibility of capillary condensation in the pores.

Preparation of the modified-coal fly ash sample

The oxidized form of coal fly ash was converted in the following way: the fly ash was treated with a 30% solution of H_2O_2 at a solution ratio to fly ash of 10:1 of weight. The activation was carried out into closed round-bottomed flask reflux condenser and mixed for 12 hours at 100°C. After modification H_2O_2-treated fly ash (FA-H_2O_2) was obtained.

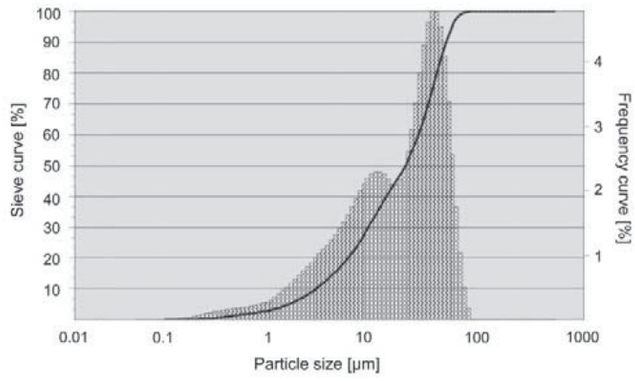

Fig. 1. The average size distribution of FA from laser analyser

Crystal violet and Cu(II) ions

Crystal violet (CV) dye, which is also known as methyl violet 10B, basic violet or 3(N-[4-[bis[4-dimethyl-amino]--phenyl]-methylene]-2,5-cyclohexadien-1-ylidine]-N-methyl--methanaminium chloride) , was used. The CV concentration in solutions was analysed spectrophotometrically at 595 nm wavelength.

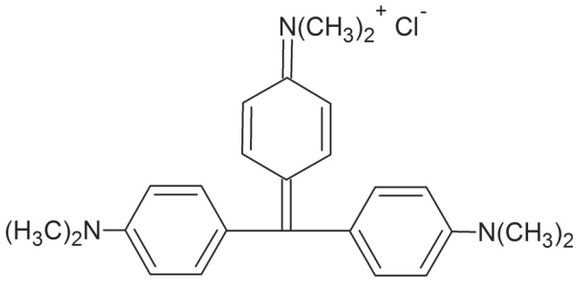

The flame atomic absorption spectrometry (FAAS) method determined the concentration of Cu(II) ions in the solution after sorption. All analytical determinations were carried out three times. By diluting stock solution of 1000 mg·L^{-1} Cu(II), the calibrant solution containing 0.0; 1.0; 2.0; 4.0; 5.0 mg·L^{-1} Cu(II) ions was prepared.

Results and discussion

Comparison of physical and chemical properties of FA with FA-H_2O_2

Chemical composition and surface morphology

Scanning electron micrographs (SEM) show the surface morphology of raw FA (Fig. 2a) and activated FA-H_2O_2 (Fig. 2b). The SEM image of raw FA shows that the fly ash particles are generally spherical in shape (Fig. 2a). From the morphological point of view the analysed raw FA, which occurs in the form of small, spherical grains, consists mainly of mixed aluminosilicates and calcium. According to (Styszko-Grochowiak et al. 2004) the unburned carbon particles are large and formed in irregulars grains. The pores are clearer and randomly located at the surface (Aslam et al. 2015). The pictograph of FA-H_2O_2 (Fig. 2b) indicated that the modification process by H_2O_2 did not lead to crystallization and was attached to the FA surface. The activation has a significant influence on the porosity development and all the particles contain micro- and mesopores (Aslam et al. 2015). The samples were detected in SEM equipped for energy-dispersive x-ray spectroscopy (EDS). For detection of the elemental composition of FA and FA-H_2O_2 an analysis of the x-ray signals was used (Fig. 2). After a chemical treatment with hydrogen peroxide the increase of oxygen content is owed to oxidation of fly ash. In order to determine the percentage of carbon and oxygen, a spot analysis of a selected sample was carried out. Oxygen to carbon ratio shows the degree of oxidation after the activation process. Post treatment of FA with H_2O_2 leads to oxidation of carbon at the surface. The increase of O/C ratio in FA-H_2O_2 in comparison to raw FA supports this fact. The increase of O/C ratio from 10.8 to 21.2 (Fig. 2) confirmed it. The presence of quartz, mullite and magnetite (Szala et al. 2015) (Fig. 3) is shown by the XRD pattern of the FA and FA-H_2O_2. The diffraction pattern of the FA-H_2O_2 indicated that the amounts of mineral in the FA-H_2O_2 increased in comparison to FA (higher than that of FA), as was observed in the height of these peak intensities.

Spectroscopic measurements (FT-IR)

In the spectra of FA and FA-H_2O_2 there was observed absorption broadband at 3440 cm^{-1}, band at 1630 cm^{-1} and absorption broadband at about 1050 cm^{-1} (Fig. 4). The band in the region 3500–3000 cm^{-1} is assigned to the stretching (-OH) and bending (H-O-H) vibrations of water molecules (Deng and Yu 2012) adsorbed on the fly ash surface (Deng and Yu 2012).

Two consecutive, very weak signals for FA-H_2O_2 at 2920 and 2850 cm^{-1} indicated that the -OH groups bound to aliphatic compounds correspond, respectively, to asymmetric and symmetric C-H stretching. The band at 1630 cm^{-1} related to bending vibrations of water molecules. The 1450 cm^{-1} band in FA and FA-H_2O_2 may be attributed to aromatic CH and carboxyl-carbonate structures (Deng and Yu 2012). The highest intensity of bands in the spectrum of researched samples is in the field of 1050 cm^{-1} and can be described as asymmetric stretching vibrations of bridge bounds ν_{as} Si-O-Si and ν_{as} Si-O-Al, occurring in tetrahedral or aluminium- and silicon-oxygen bridges, typical for aluminosilicates framework structures (Mozgawa et al. 2006). What can be observed is the increase of band intensity in the field of 3440 cm^{-1} in the spectrum of FA-H_2O_2. Coal fly ash oxidized with H_2O_2 was more hydrophilic than that of the corresponding unoxidized

sample. The presence of polar groups on the surface is likely to provide considerable cation exchange capacity to the adsorbents. The surface structures of carbon-oxygen (functional groups) are by far the most important structures in influencing the surface characteristics and surface behaviour of FA-H_2O_2. The bands appearing at about 800 cm^{-1} are associated with symmetric stretching vibration of quartz present in the as-received FA in form Al,Si-O. The spectra FA and FA-H_2O_2 contain a characteristic doublet of quartz at 798 and 780 cm^{-1}. Furthermore, the symmetrical stretching variation at 730 cm^{-1} and symmetrical stretching variation at 660 cm^{-1} associated with Si-O-Al and Si-O-Si appropriate were suggested by Mozgawa et al. 2006. Pseudolattice vibrations, originating from overtetrahedral structural units and the double ring of secondary building unit (SBU) can be observed to be present in the zeolite structure in the FA (rings made of siliconoxygen and aluminiumoxygen tetrahedra), corresponding to infrared frequency, and equal to 550 cm^{-1}. Moreover, the band at about

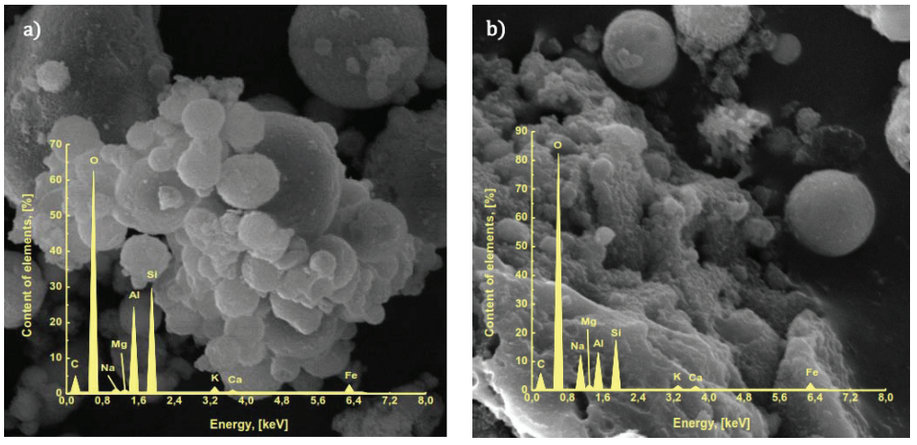

Fig. 2. SEM images and EDS spectrum of the coal fly ash; a) the raw FA and b) the H_2O_2 treated FA

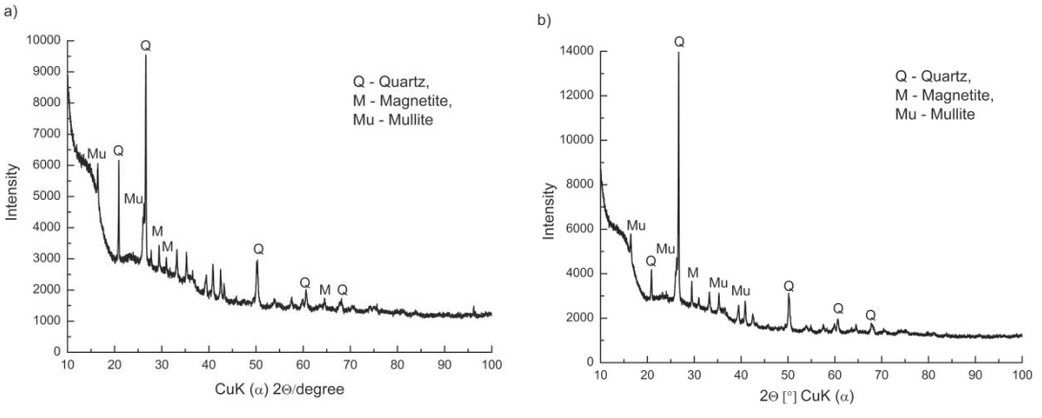

Fig. 3. XRD patterns of a) the raw FA and b) the H_2O_2 treated FA

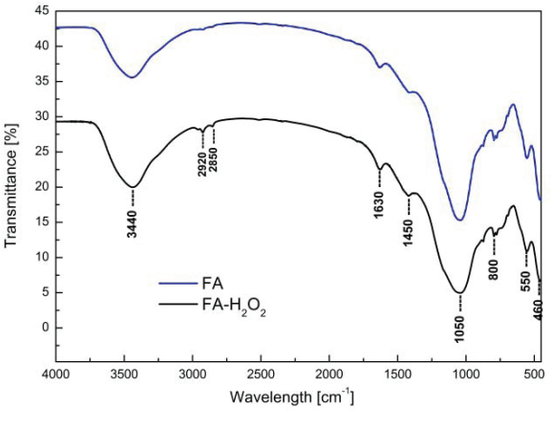

Fig. 4. FT-IR spectra of raw FA and H_2O_2 treated FA

550 cm^{-1}correspond to symmetric stretching vibrations of ν_s Si-O-Si bridge bonds and bending vibrations of δ O-Si-O as complex band (Mozgawa et al. 2006). Based on the FT-IR spectrum, the presence of pore openings corresponding to the band at 460 cm^{-1} in the FA and FA-H_2O_2 can be observed, which can be attributed to the dissolution of the minerals (viz., quartz and mullite) present in the samples.

Thermal gravimetric analysis

The curves of the differential thermal analysis (DTA) and thermogravimetric analysis (TG) of the FA sample, shown in Fig. 5a, present a small mass loss in the temperature range from 50°C to 150°C, which is caused by evaporation of water from the FA (Table 1). This endothermic process for FA is assigned to the dehydration/thermodesorption of water ca. 0.2% (Aslam et al. 2015). The registered mass change in the temperature range from 250°C to 400°C indicated that exothermic process is related to oxidation of residue of organic matter of about 7.4%. A larger mass loss in the temperature range of 400–600°C is caused by dehydration of calcium hydroxide (endothermic process) and decomposition of calcium carbonate (exothermic process). The next dehydration process corresponds to the loss of coordinated and structural -OH groups of water (peak at 520°C). This endothermic peak is assigned to the dehydroxylation of FA, i.e. the removal of hydroxyl groups from tetrahedral structural units. The next exothermic peak at the temperature of 600°C indicates recrystallization process. The last stage in the temperature range from 650°C to 800°C was endothermic decomposition of the mineral structure. The total mass loss during the process amounted to 8%. The differential thermal analysis of FA-H_2O_2 indicated (Fig. 5b) that in the temperature range of 300–600°C it is an endothermic process, which is caused by the decomposition of calcium hydroxide, calcium carbonate and oxygen functional groups on the sample surface (Table 1).

Sorption studies

The adsorption experiments of CV and Cu(II) onto modified coal fly ash were conducted in batch method, which permits the complete evaluation of parameters that influence the process of adsorption. In this method, a series of 100 mL glass flasks were filled with 50 mL CV or Cu solution (in single component system) and 50 mL CV and Cu solution (in bi-component system) of varying concentrations (10–500 $mg \cdot L^{-1}$). The adsorption kinetic experiments were conducted at room temperature using the solution at concentrations of 50 $mg \cdot L^{-1}$ at pH 9 and mixed at 190 rpm. The rate of CV and Cu uptake was then measured by taking samples at various time intervals for five hours. Then 0.5 g of FA/FA-H_2O_2 was added into each flask and subjected for agitation until equilibrium was attained after 2 hours. The resultant solutions were centrifuged and supernatant liquids were subjected for the determination of CV and Cu.

Error analysis

In order to quantitatively compare the applications of each model, the coefficients of determination (R^2) and a reduced chi-square test (χ^2/DoF) were calculated (Wang 2012). The

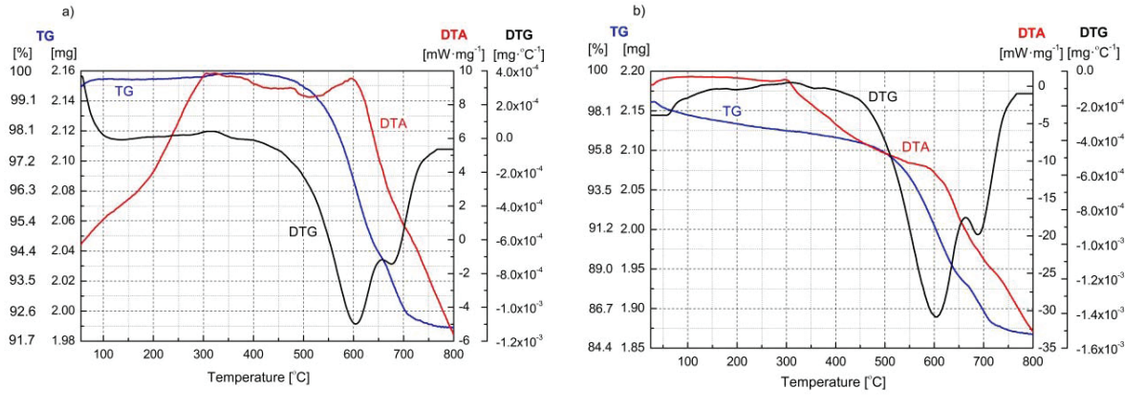

Fig. 5. DTA, TG and DTG curves of FA (a) and FA-H_2O_2 (b)

Table 1. Changes of FA and FA-H_2O_2 properties, which occurred as a result of heating during the thermogravimetric analysis

Kind of process	Type of reaction	Range of reaction temperature [°C]
Evaporation of water (moisture, hydration water)	Endothermic	50–150
Oxidation of residue of organic matter	Exothermic	250–400
Dehydration of calcium hydroxide	Endothermic	400–600
Decomposition of calcium carbonate	Exothermic	
Dehydration of coordinated and structural of water/dehydroxylation of FA and FA-H_2O_2	Endothermic	520
Recrystallization	Exothermic	600
Decomposition of mineral structure	Endothermic	650–800

linear and non-linear regression (reduced chi-square) value was calculated by using Origin Pro 7.5 software:

$$\chi^2 / \mathrm{DoF} = \frac{1}{\mathrm{DoF}} \sum_{i=1}^{N} \frac{(q_{ei} - q_{ei,m})^2}{q_{ei,m}}$$

where DoF, q_{ei} and $q_{ei,m}$ are degrees of freedom, experimental data and model data. The error bars in the line graph represent a confidence interval of t-distribution; the significance was set at p = 95% and n = 3.

Kinetic studies

The kinetic rate constants were calculated by using pseudo--first-order (PFO) (Ho 2004), pseudo-second-order (PSO) (Ho 2006) kinetic models, whereas Weber and Morris model (intra-particle diffusion model) helped to determine the rate controlling stage (Cabal et al. 2009). Table 2 presents the values of these parameters. The kinetic sorption experimental data fit by using nonlinear PFO and PSO equations were performed. The values of the reduced chi-square test and the coefficient of determination in the PSO model (χ^2/DoF = 0.08; R^2 = 0.980) were slightly lower for Cu(II) than those of the PFO model (χ^2/DoF = 0.15; R^2 = 0.964), what is an indication that the PSO model is better than the PFO model. The PSO model is based on the assumption that the chemisorption occurs (Ho 2006). The kinetic sorption experimental data fit by using nonlinear PFO and PSO equations are shown in Fig. 6a. The initial adsorption rate $u = k_2 qe^2$, can be calculated from the PSO rate of equation. Obtained initial adsorption rate for Cu(II) and CV was done 1.1 and 0.4 [mg·g^{-1}·min^{-1}] respectively. It was found that adsorption rate of Cu(II) was higher compared to CV on FA-H_2O_2.

The multilinear plots of Weber and Morris equation $qt = k'_i t^{1/2} + bi$ were indicated two separate regions for adsorption of Cu(II) and CV (Alver and Metin 2012). The comparison of the micropore diffusion constant k'_2 values for Cu(II) and CV showed that they were lower than those for the macropore diffusion constants k'_1 of 0.43 and 0.64, respectively for Cu(II) and CV (Fig. 6b). Furthermore, the rate of micropore diffusion is a slower step than determining rate step (Cabal et al. 2009). The film diffusion effect (second line from the plots of qt versus $t^{1/2}$) shows greater effect on the micropore diffusion stage (4.8 and 4.3), respectively for Cu(II) and CV, than in the macropore stage, where it is close to zero.

pH influence

The effect of pH values on the sorption of Cu(II) and CV onto FA-H_2O_2 was studied for pH values of 2–11 (Fig. 7). It was found that at pH 9.0 the sorption percentage of FA-H_2O_2

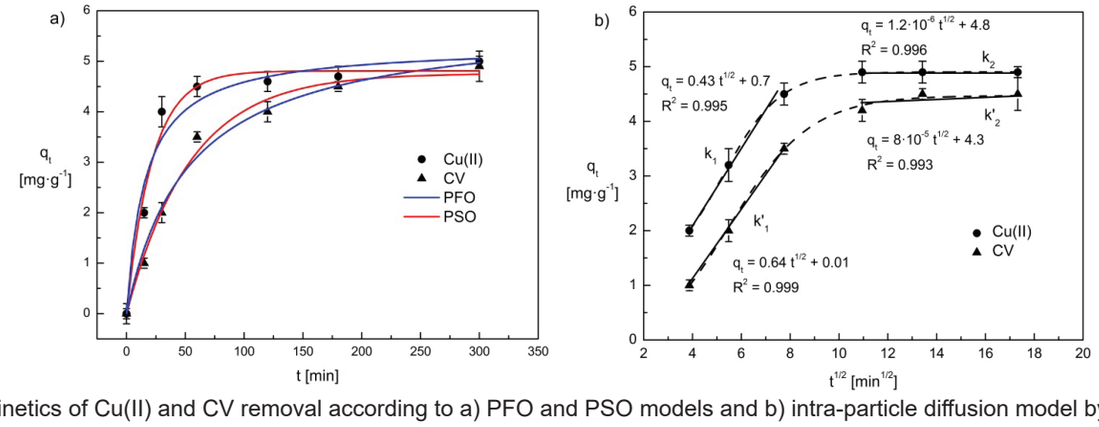

Fig. 6. Kinetics of Cu(II) and CV removal according to a) PFO and PSO models and b) intra-particle diffusion model by FA-H_2O_2

Table 2. Kinetic model constants and correlation coefficients for the sorption systems

Kinetic model	Equation	Parameter	Cu(II)	CV
Pseudo-first-order (PFO)	$dq/dt = k_1(q_e - q_t)$ $q_t = q_e (1 - e^{-k1t})$	χ^2/DoF R^2 k_1 [min^{-1}] q_e [mg·g^{-1}]	0.15 0.964 $1.2 \cdot 10^{-2}$ 5.3	0.05 0.987 $3.2 \cdot 10^{-3}$ 5.8
Pseudo-second-order (PSO)	$dq/dt = k_2(q_e - q_t)^2$ $q_t = k_2 q_e^2 t/(1 + k_2 q_e t)$	χ^2/DoF R^2 k_2 [g·mg^{-1}·min^{-1}] q_e [mg·g^{-1}]	0.08 0.980 $4.6 \cdot 10^{-2}$ 4.8	0.04 0.990 $1.8 \cdot 10^{-2}$ 4.8
Intra-particle diffusion	$q_t = k'_i t^{1/2} + b_i$	R^2 k'_1 [mg·g^{-1}·min$^{-1/2}$] b_1 [mg·g^{-1}]	0,995 0.43 0.7	0.999 0.64 0.01
		R^2 k'_2 [mg·g^{-1}·min$^{-1/2}$] b_2 [mg·g^{-1}]	0.996 $1.2 \cdot 10^{-6}$ 4.8	0.993 $8 \cdot 10^{-5}$ 4.3

for Cu(II) ions and CV was 99% for Cu(II) and 80% for CV, respectively. The order of affinity based on the amount of sorbate removal is as follows: Cu(II) > CV.

The order of affinity is due to the fact that a different sorbate will experience different physical and electrostatic forces according to their molecular size. Coal fly ash oxidized by H_2O_2 has more oxygen surface of the tetrahedral sheet than that of the corresponding unoxidized sample. The presence of polar groups on the surface of FA-H_2O_2 is likely to give considerable cation exchange capacity to the sorbents. At high pH the solution in contact with the FA-H_2O_2 contains excess hydroxyls. It was found that electrostatic attraction between a negatively charged silanol group and positively charged CV molecule predominates the sorption process. In the higher range of pH, the FA-H_2O_2 surface has negative charge. Basically, crystal violet produced molecular cations (C^+) and reduced ions (CH^+). With the increasing solution pH, the sorption capacity increases due to weaker forces of repulsion between the FA-H_2O_2 and CV. Moreover, the combined process of precipitation ($Cu(OH)_2$) and adsorption ($Cu(OH)_3^-$, $Cu(OH)_4^{2-}$) at pH > 9 was observed (Sočo and Kalembkiewicz 2015). The Cu(II) ions and CV dye sorption are attributed to different mechanisms of the ion-exchange processes as well as to the adsorption. Thus, favorable pH for sorption of cationic dye, such as CV and Cu(II) ions, will be greater than pH 9. The mechanism of Cu(II) ions and CV dye sorption includes ion-exchange, surface adsorption process and also dissolution--reprecipitation in the case of Cu(II), as shown in Fig. 8.

Adsorption isotherms in single-component system

Freundlich isotherm is generally applied to describe heterogeneous surface. The obtained values of *1/n* (0.48 and 0.85) while *n* (2.1 and 1.2) showed the favourable nature of Cu(II) and CV sorption onto FA-H_2O_2 and the heterogeneity of the sorbent sites at the studied temperature (Alver and Metin 2012; Liu and Zhang 2015). Equilibrium experiments show that the Cu(II) ions have the smallest hydrated ionic radii (4.19Å) and have tendency to move faster to potential adsorption sites on FA-H_2O_2, when compared to the CV cations with higher ionic radii (Sočo and Kalembkiewicz 2015).

In order to describe the adsorption of solutes from liquid solutions Langmuir isotherm is often used and the model assumes monolayer adsorption onto a homogeneous surface with a finite number of identical sites (Liu and Zhang 2015). Table 3 presents the adsorption parameters obtained from this model. The maximum monolayer adsorption capacity *qmax* of the FA-H_2O_2 was not affected at pH 9, but decline at lower pHs was found to be 112.5 and 21.2 mg·g^{-1} for Cu(II) and CV respectively.

Redlich-Peterson (R-P) isotherm contains three parameters and is an improvement over the Langmuir and Freundlich isotherms. It can be applied in homogenous as well

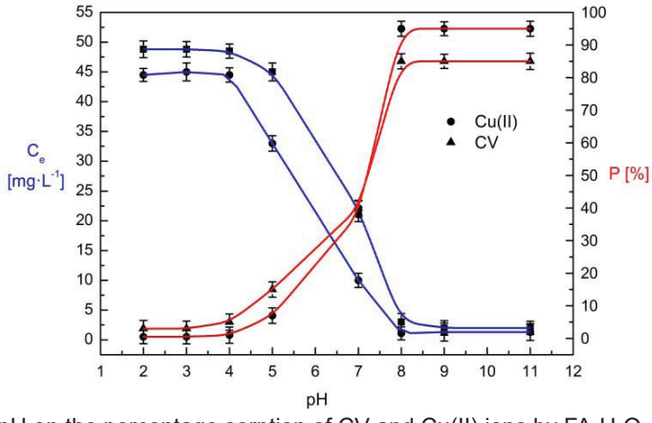

Fig. 7. Effect of solution pH on the percentage sorption of CV and Cu(II) ions by FA-H_2O_2 at T = 293 K and t = 2 h

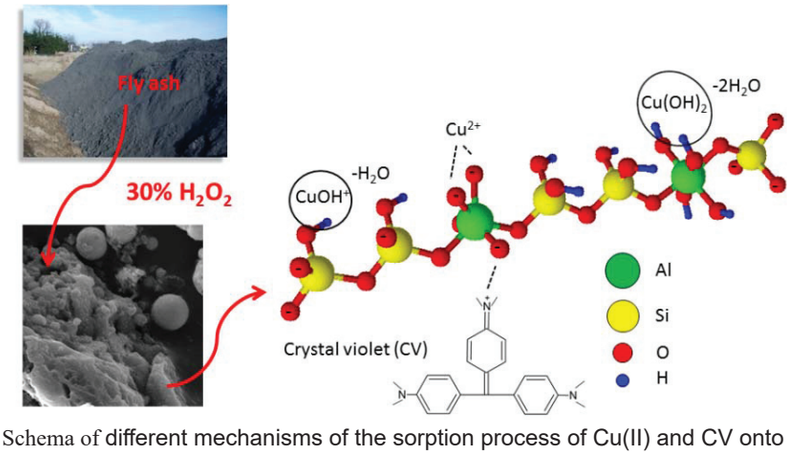

Fig. 8. Schema of different mechanisms of the sorption process of Cu(II) and CV onto FA-H_2O_2

as heterogeneous systems (Bedin et al. 2016). Examination of the data showed that the R-P isotherm was an appropriate description of the data for Cu(II) sorption on the FA-H_2O_2 in the studied concentration range (χ^2/DoF = 0.05; R^2 = 0.999). The R-P constant *B* normally varies between 0 and 1, indicating favorable adsorption. At high concentration (*B→0)* the R-P model approaches Freundlich isotherm and in accordance with low concentration (*B→1)* it approaches Langmuir isotherm. As it can be noticed in Table 3, the value of *B* was in this range (0.79) only for Cu(II). The adsorption sequence is found to be in the order of increasing molecular weight, i.e. Cu(II) > CV.

The model of adsorption surface considered by Jovanović (Ghanabari Pakdehi and Alipour 2013) is essentially the same as that considered by Langmuir. Fig. 9d shows the comparison between the experimental data and Jovanović. The values for the Jovanović model were lower than in all other models.

The equation defining the Elovich (Hamdaouia and Naffrechoux 2007) model is based on a kinetic principle assuming that the adsorption sites increase exponentially with adsorption, which implies multilayer adsorption. As shown in Fig. 9f and Table 3, the values of the regression coefficient R^2 are lower than those of Langmuir, R-P and Tóth; therefore the adsorption of Cu(II) and CV on FA-H_2O_2 does not fit the Elovich isotherm.

The Halsey equation (Gholitabar and Tahermansouri 2017) is suitable for multilayer adsorption and fitting of the experimental data to this equation proves heteroporous nature of adsorbent. The values of for the Halsey model are significantly dominant in comparison to other models, what suggests that the Halsey model could not describe the experimental data satisfactorily for the adsorption of Cu(II) and CV on FA-H_2O_2. This result also shows that the adsorption of Cu(II) and CV on FA-H_2O_2 was not based on significant multilayer adsorption.

Brunauer-Emmett-Teller (BET) isotherm is a theoretical equation, most commonly applied in the gas–solid equilibrium systems, but its extended model can be also related to liquid–solid interface (Foo and Hameed 2010).

The Tóth isotherm model has been applied for the modelling of several multilayer and heterogeneous adsorption systems. The parameter *Th* characterizes the heterogeneity of the adsorption system (Ho et al. 2002) and when *Th* = 1, this equation reduces to Langmuir isotherm equation. The application of this isotherm is best suited to multilayer adsorption similar to BET isotherms (Hamdaouia and Naffrechoux 2007).

The BET and Tóth model is also not suitable in describing adsorption of Cu(II) and CV on FA-H_2O_2, because this model also assumes multilayer behavior of the adsorption of adsorbate onto adsorbent. This is in compliance with large and R^2 values.

Sorption of Cu(II) ions in a single system by means of FA-H_2O_2 was well fitted by Langmuir and R-P models. Comparing the values of χ^2/DoF received for Cu(II) of the considered isotherms, the fitting degree follows the immediate sequence: R-P ≈ Langmuir > Jovanović > Freundlich > Tóth > BET > Elovich > Halsey. Comparing the R^2 values, similar sequence was observed. The Langmuir and R-P isotherms provide precise representation over the range of experimental conditions studied, though the R-P model performs slightly better by low value of reduced chi-square test (0.05) and high coefficient of determination (0.999).

The Jovanović and Langmuir isotherms were used to fit the experimental equilibrium of CV dye sorption. Comparing the values of the reduced chi-square test and the determination coefficient obtained for CV of the considered isotherms, the fitting degree follows the sequence: Jovanović > Langmuir > Elovich > Freundlich > R-P > Tóth > Halsey > BET.

On the basis of Halsey and BET isotherms, higher error of calculated values, in comparison to experimental data, was found. The studied equations are suitable for multilayer adsorption and the fitting of the experimental data to these equations proves the heteroporous nature of the adsorbent. The obtained high error (> 80) demonstrates that the sorption of Cu(II) ions and CV dye onto FA-H_2O_2 cannot describe the experimental data satisfactorily multilayer sorption.

Adsorption isotherms in bi-component system

Estimation of sorption isotherm parameters in a bi--component system of Cu(II)-CV showed that the best fit of the values calculated for experimental data for both sorbates have been displayed by the extended Langmuir model (EL) (Al--Asheh et al. 2000), and Jain-Snoeyink model (JS) (Noroozi and Sorial 2013), but only in the case of CV dye (Fig. 10, Table 4).

Figs. 11a and b show the comparison of the experimental adsorption data of Cu(II) and CV onto FA-H_2O_2 and the calculated *qe* values in Cu(II)-CV system, by means of bi-component isotherm models which were mentioned before. The dissimilarity in values of the system of Cu(II)-CV between the experimental and calculated values for the entire data set of Cu(II) and CV are given in Fig. 11. If most of the data points were placed around the 45° line, then the studied isotherm models could well represent the experimental adsorption data of the bi-component systems (Al-Asheh et al. 2000; Vieira et al. 2007).

The EL model fitted well to the bi-component adsorption data of Cu(II) and CV onto FA-H_2O_2 and can be satisfactorily used to estimate equilibrium data, respectively, from the single isotherm parameters. The JS model poorly fitted the equilibrium data and could not be used to forecast the binary--system adsorption because in this case there were many points lying far away from the 45° line, rather than being placed around this line (Al-Asheh et al. 2000). The values of the indicated that the ELF bi-component isotherm fitted worst the experimental data with the highest reduced chi-square test of 35.2 and 41.5, respectively for Cu(II) and CV, in comparison to other investigated models. The explanation of the results is that the isotherm does not incorporate any parameter accounting for the interactions between metal ion and cationic dye. The EL bi-component isotherm approximated reasonably well the experimental data since the isotherm provided of 0.6 and 0.5 respectively for Cu(II) and CV.

The adsorption experimental points in a bi-component Cu(II)-CV onto FA-H_2O_2 system and the three-dimensional graphical surface plot (Medellin-Castillo et al. 2017; Padilla--Ortega et al. 2013) forecast by the EL model are shown in Figs. 12a and b. Furthermore, the forecast of equilibrium data points with the isotherm using the EL model was found to be satisfactory. This model was calculated as the best fit for bi-component adsorption models based on the EL isotherm for modeling the binary adsorption of Cu(II) ions and CV dye from aqueous solutions onto FA-H_2O_2 because it uses the single Langmuir isotherm parameters (Medellin-Castillo et al. 2017; Padilla-Ortega et al. 2013).

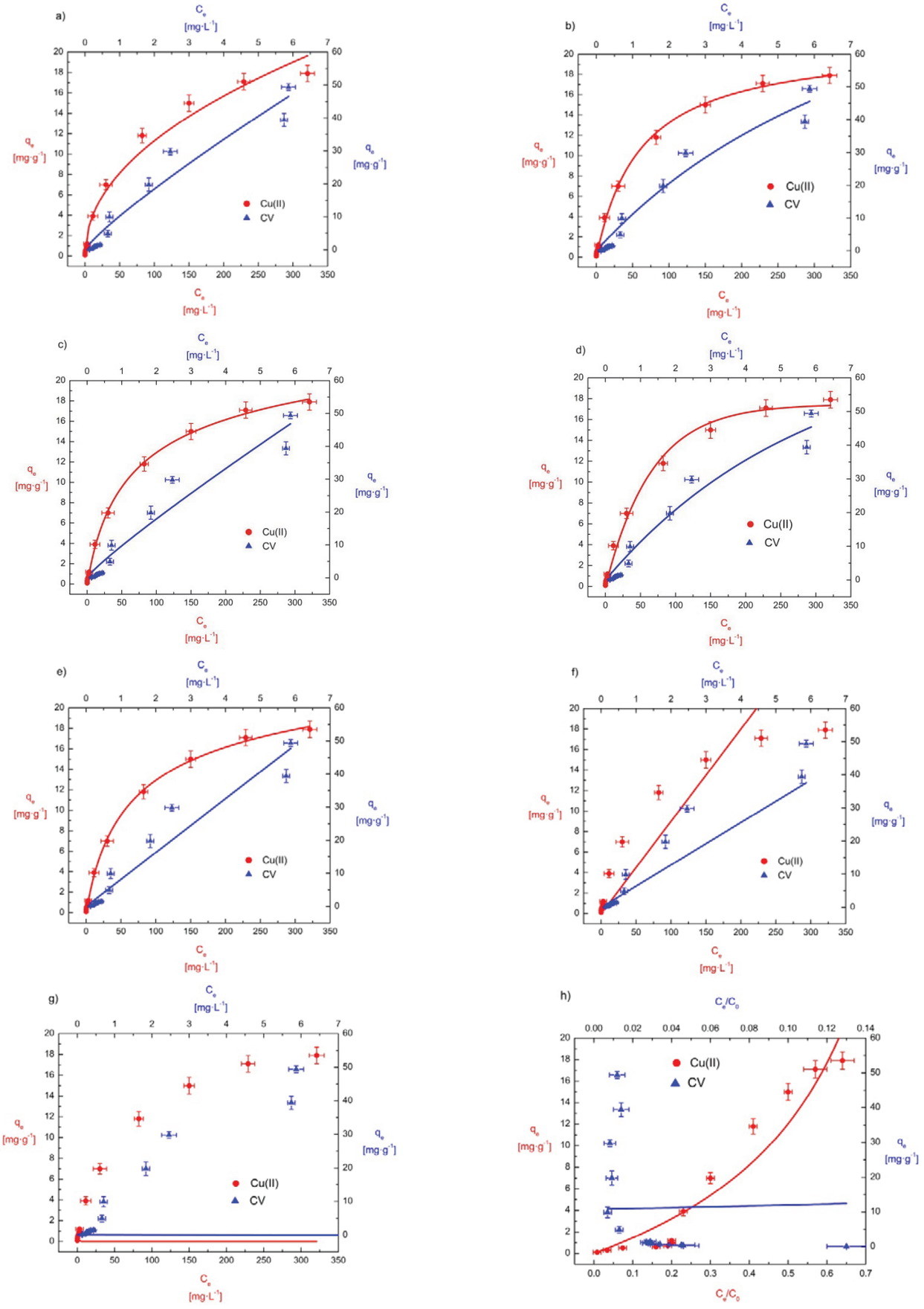

Fig. 9. Plot of isotherm models a) Freundlich, b) Langmiur, c) R-P, d) Jovanović, e) Tóth, f) Elovich, g) Halsey, h) BET in a single-component syste

Table 3. Parameter values of the single adsorption isotherms for removal Cu(II) and CV by FA-H_2O_2

Isotherm model	Equation	Parameter	Cu(II)	CV
Freundlich	$q_e = K_F C_e^{1/n_F}$	K_F $mg^{1-1/n} \cdot L^{1/n} \cdot g^{-1}$	1.3	10.2
		n_F	2.1	1.2
		χ^2/DoF	1.0	14.4
		R^2	0.981	0.952
Langmuir	$q_e = q_{max} \frac{K_L C_e}{1 + K_L C_e}$	K_L $L \cdot mg^{-1}$	0.1	0.02
		q_{max} $mg \cdot g^{-1}$	112.5	21.2
		χ^2/DoF	0.08	11.1
		R^2	0.998	0.963
Redlich and Peterson	$q_e = \frac{K_{RP} C_e}{1 + a_{RP} C_e^B}$	K_{RP} $L \cdot g^{-1}$	0.43	0.08
		a_{RP} $(L \cdot mg^{-1})^B$	0.04	$2 \cdot 10^{-6}$
		B	0.79	10^{-3}
		χ^2/DoF	0.05	16.4
		R^2	0.999	0.845
Jovanović	$q_e = q_{max} (1 - \exp(-K_J C_e))$	K_J $L \cdot mg^{-1}$	0.015	0.174
		q_{max} $mg \cdot g^{-1}$	17.5	71.0
		χ^2/DoF	0.3	10.8
		R^2	0.994	0.964
Tóth	$q_e = \frac{q_{max} K_{Th} C_e}{[1 + (K_{Th} C_e)^{Th}]^{\frac{1}{Th}}}$	q_{max} $mg \cdot g^{-1}$	0.02	0.004
		K_{Th} $(L \cdot mg^{-1})^{Th}$	14.9	0.4
		Th	0.9	10^{-4}
		χ^2/DoF	3.5	18.9
		R^2	0.963	0.942
Elovich	$q_e = q_{max} K_E C_e \exp(-\frac{q_e}{q_{max}})$	K_E $L \cdot mg^{-1}$	0.03	0.81
		q_{max} $mg \cdot g^{-1}$	3.1	8.1
		χ^2/DoF	44.2	8.1
		R^2	0.647	0.885
Halsey	$q_e = (\frac{K_H}{C_e})^{1/n_H}$	K_H $mg^{n+1} \cdot g^{-1} \cdot L^{-1}$	0.011	0.015
		n_H	2.3	0.9
		χ^2/DoF	87.1	88.3
		R^2	< 0.1	< 0.1
Brunauer, Emmett and Teller	$q_e = q_{max} \frac{K_{BET} \frac{C_e}{C_0}}{(1 - \frac{C_e}{C_0})[1 + (K_{BET} - 1)\frac{C_e}{C_0}]}$	K_{BET}	1.24	2.80
		q_{max} $mg \cdot g^{-1}$	10.9	10.8
		χ^2/DoF	4.6	304.7
		R^2	0.909	< 0.1

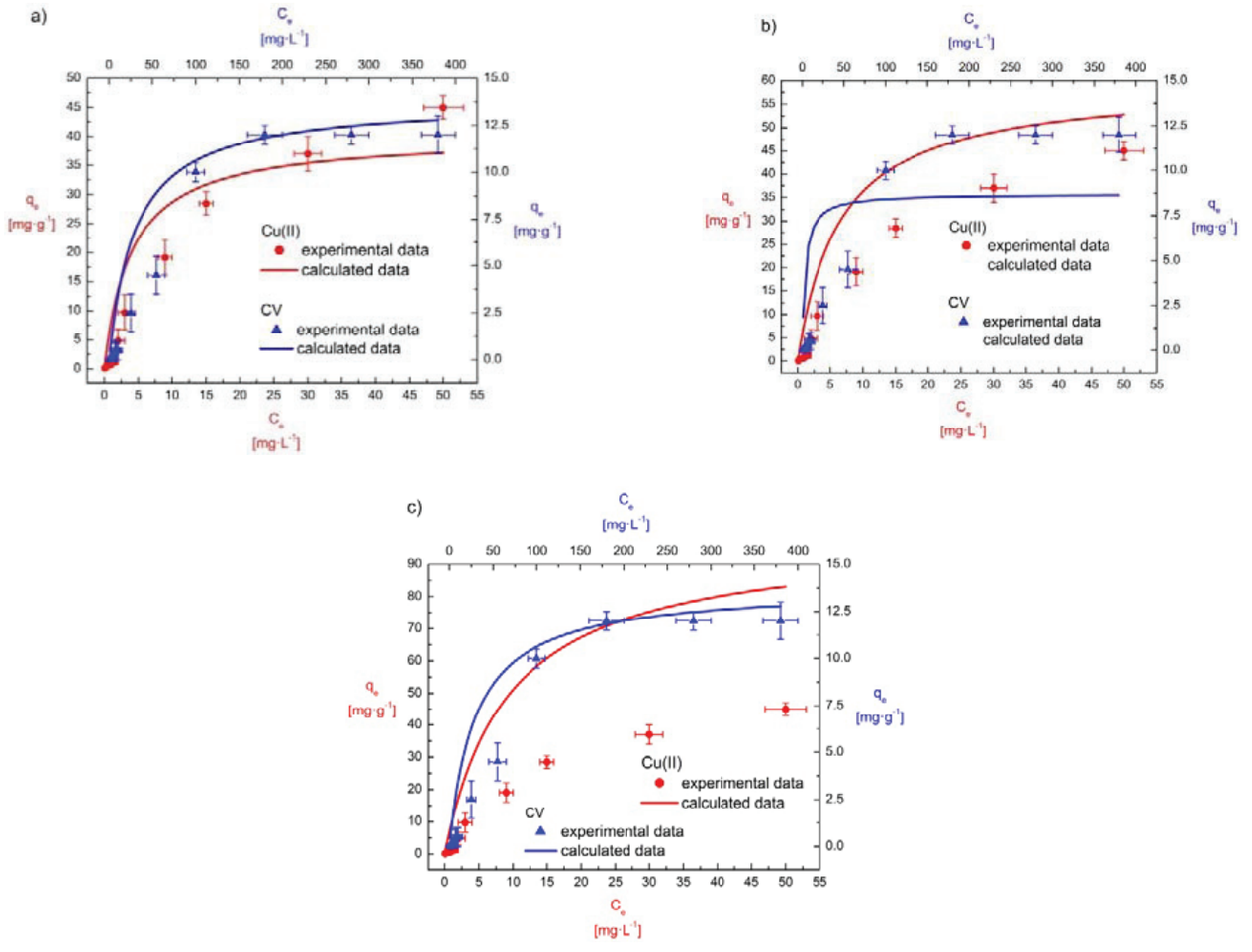

Fig. 10. Estimation of Cu(II)-CV adsorption in a bi-component system using a) EL, b) ELF, c) JS isotherm models

Table 4. Parameter values of the bi-component isotherms for the Cu(II)-CV on FA-H_2O_2

Isotherm model	Equation	Parameter	Cu(II)	CV
Extended Langmuir	$q_{ei} = q_{maxi}\frac{K_{Li}C_{ei}}{1+\sum_{j=1}^{N} K_{Lj}C_{ej}}$	χ^2/DoF	0.6	0.5
		R^2	0.981	0.991
Extended Langmuir and Freundlich	$q_{ei} = q_{maxi}\frac{(K_{Li}C_{ei})^{1/n_i}}{1+\sum_{j=1}^{N} (K_{Lj}C_{ei})^{1/n_j}}$	χ^2/DoF	35.2	41.5
		R^2	0.471	0.586
Jain and Snoeyink	$q_{e1} = (q_{max1} - q_{max2})\frac{K_{L1}C_{e1}}{1+K_{L1}C_{e1}} + q_{max2}\frac{K_{L1}C_{e1}}{1+K_{L1}C_{e1}+K_{L2}C_{e2}}$ when $q_{max1} > q_{max2}$ $q_{e2} = q_{max2}\frac{K_{L2}C_{e2}}{1+K_{L1}C_{e1}+K_{L2}C_{e2}}$	χ^2/DoF	37.3	0.02
		R^2	0.325	0.997

In this plot, the removal experimental points of Cu(II) and CV are shown together with the forecast isotherm using the EL isotherm. Fig. 12a shows the removal process of Cu(II) in the presence of CV, and in the range of CV concentration from 0 to 400 mg·L^{-1}. The removal of Cu(II) declined sharply while increasing the concentration of CV at equilibrium. In Fig. 12b the dependence of Cu(II) concentration on the removal of CV is shown. The removal of CV was insignificantly constrained by the contest of Cu(II), and the decrease of CV removal was nearly proportional to the increase of the Cu(II) concentration.

In the competitive adsorption, the removal of Cu(II) decreased to a greater extent than that of CV. Therefore, the CV displayed strong effect in the competitive adsorption of Cu(II), whereas the Cu(II) did not influence the competitive adsorption of CV (Medellin-Castillo et al. 2017; Padilla-Ortega et al. 2013).

Conclusions

The results show that treating fly ash with H_2O_2 solution was a promising way to enhance the inhibition of Cu(II) and Crystal violet (CV) dye mobility. By comparing the values of error functions in a single-component system it was found that the R-P and Langmuir adsorption models are best to fit the Cu(II) ions onto FA-H_2O_2, whereas adsorption of CV dye is best described by Langmuir and Jovanović isotherms, respectively. A high degree of determination with low reduced chi-square values can be observed in these models. On the basis of the equilibrium data of the studied systems it was concluded that the experimental values were poorly estimated by Halsey and BET models, with high values of reduced chi-square test compared to the other isotherms, thus indicating that multilayer sorption of Cu(II) and CV dye onto FA-H_2O_2 did not come into existence. The single component system adsorption on FA-H_2O_2 showed that the capacity of FA-H_2O_2 for removing Cu(II) was 5.3 times greater than that of CV dye. The competitive adsorption in a single component system indicated that FA-H_2O_2 had stronger affect to Cu(II) than to CV dye, which is related to their hydrated ionic radius. The EL model constitutes the best interpretation for the bi-component system in the competitive adsorption of Cu(II) ions and CV dye on FA-H_2O_2. Based on the obtained adsorption capacity a conclusion may be drawn that FA-H_2O_2 can be used to treat wastewaters containing Cu(II) ions and CV dye.

Acknowledges

The X-ray analysis was carried out in the Laboratory of Spectrometry, Faculty of Chemistry, Rzeszów University of Technology, Al. Powstańców Warszawy 6., PL-959 Rzeszów, Poland and was financed from the DS budget.

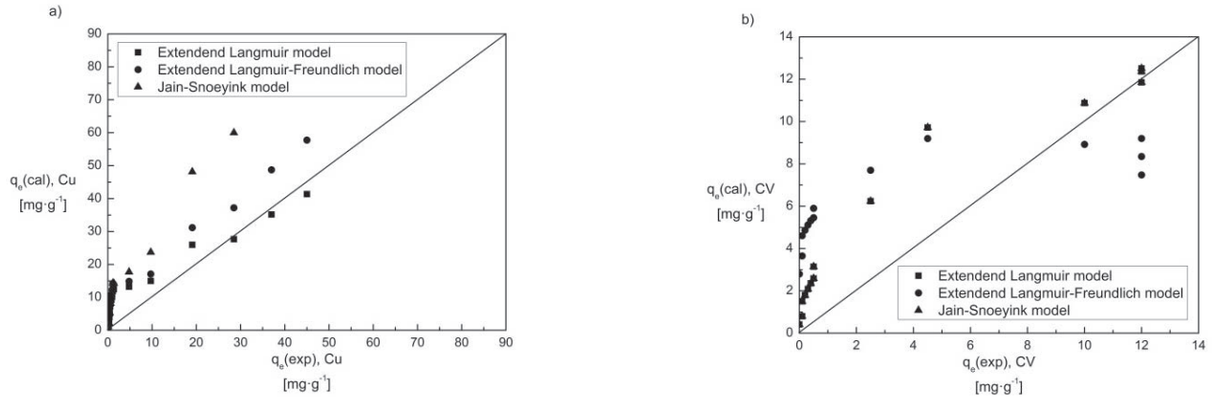

Fig. 11. The relationship between experimental and calculated sorption capacities of a) Cu(II) ions, b) CV dye in Cu-CV system

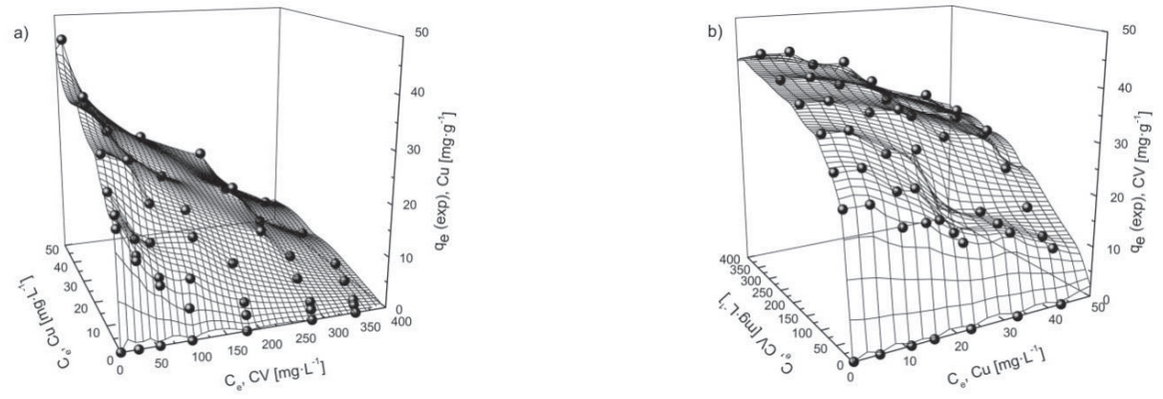

Fig. 12. Adsorption isotherms of Cu(II)-CV in bi-component system. The forecast of surfaces by the EL model a) q_e (exp) Cu(II) and b) q_e (exp) CV

References

Ahmaruzzaman, M. (2010). A review on the utilization of fly ash, *Progress Energy Combustion,* 36, pp. 327363, DOI: 10.1016/j.pecs.2009.11.003

Al-Asheh, S., Banat, F., Al-Omari, R. & Duvnjak, Z. (2000). Predictions of binary sorption isotherms for the sorption of heavy metals by pine bark using single isotherm data, *Chemosphere,* 41, pp. 659–665, DOI: 10.1016/S0045-6535(99)00497-X.

Alver, E. & Metin, A.Ü. (2012). Anionic dye removal from aqueous solutions using modified zeolite: Adsorption kinetics and isotherm studies, *Chemical Engineering Journal,* 200–202, pp. 59–67, DOI: 10.1016/j.cej.2012.06.038.

Amodu, O.S., Ojumu, T.V., Ntwampe, S.K. & Ayanda, O.S. (2015). Rapid Adsorption of Crystal Violet onto Magnetic Zeolite Synthesized from Fly Ash and Magnetite Nanoparticles, *Journal of Encapsulation and Adsorption Sciences,* 5, pp. 191203, DOI: 10.4236/jeas.2015.54016.

An, C. & Huang, G. (2012). Stepwise adsorption of phenanthrene at the fly ash-water interface as affected by solution chemistry: Experimental and modeling studies, *Environmental Science & Technology,* 46, pp. 12742–12750, DOI: 10.1021/es3035158.

Anirudhan, T.S. & Ramachandran M. (2015). Adsorptive removal of basic dyes from aqueous solutions by surfactant modified bentonite clay (organoclay): Kinetic and competitive adsorption isotherm, *Process Safety and Environmental Protection,* 95, pp. 215–225, DOI: 10.1016/j.psep.2015.03.003.

Aslam, Z., Shawabkeh, R.A., Hussein, I.A., Al-Baghli, N. & Eic, M. (2015). Synthesis of activated carbon from oil fly ash for removal of H_2S from gas stream, *Applied Surface Science,* 327, pp. 107–115, DOI: 10.1016/j.apsusc.2014.11.152.

Bedin, K.C., Martins, A.C., Cazetta, A.L., Pezoti, O. & Almeida, V.C. (2016). KOH-activated carbon prepared from sucrose spherical carbon: Adsorption equilibrium, kinetic and thermodynamic studies for Methylene Blue removal, *Chemical Engineering Journal,* 286, pp. 476–484, DOI: 10.1016/j.cej.2015.10.099.

Cabal, B., Ania, C.O., Parra, J.B. & Pis, J.J. (2009). Kinetics of naphthalene adsorption on an activated carbon: Comparison between aqueous and organic media, *Chemosphere,* 76, pp. 433–438, DOI: 10.1016/j.chemosphere.2009.04.002.

Canpolat, F., Yilmaz, K., Kose, M.M., Sumer, M. & Yurdusev, M.A. (2004). Use of zeolite, coal bottom ash and fly ash as replacement materials in cement production, *Cement and Concrete Research*, 34, pp. 731–735, DOI: 10.1016/S0008-8846(03)00063-2.

Dai, S., Ren, D., Chou, C.-L., Finkelman, R.B., Seredin, V.V. & Zhou, Y. (2012). Geochemistry of trace elements in Chinese coals: A review of abundances, genetic types, impacts on human health, and industrial utilization, *International Journal of Coal Geology,* 94, pp. 3–21, DOI: 10.1016/j.coal.2011.02.003.

Deng, H. & Yu, X. (2012). Adsorption of fluoride, arsenate and phosphate in aqueous solution by cerium impregnated fibrous protein, *Chemical Engineering Journal,* 184, pp. 205–212, DOI: 10.1016/j.cej.2012.01.031.

Foo, K.Y. & Hameed, B.H. (2010). Insights into the modeling of adsorption isotherm systems, *Chemical Engineering Journal,* 156, 2–10, DOI: 10.1016/j.cej.2009.09.013.

Franus, W., Wiatros-Motyka, M.M. & Wdowin, M. (2015). Coal fly ash as a resource for rare earth elements, *Environmental Science and Pollution Research,* 22, pp. 9464–9474, DOI 10.1007/s11356-015-4111-9

Gholitabar, S. & Tahermansouri, H. (2017). Kinetic and multi--parameter isotherm studies of picric acid removal from aqueous solutions by carboxylated multi-walled carbon nanotubes in the presence and absence of ultrasound, *Carbon Letters,* 22, pp. 14–24, DOI: 10.5714/CL.2017.22.014.

Gupta, V.K. & Suhas (2009). Application of low-cost adsorbents for dye removal e a review, *Journal of Environmental Management,* 90, pp. 2313–2342, DOI: 10.1016/j.jenvman.2008.11.017.

Hamdaouia, O. & Naffrechoux, E. (2007). Modeling of adsorption isotherms of phenol and chlorophenols onto granular activated carbon Part I. Two-parameter models and equations allowing determination of thermodynamic parameters, *Journal of Hazardous Materials,* 147, pp. 381–394, DOI: 10.1016/j.jhazmat.2007.01.021.

Ho, Y.S. (2004). Citation review of Lagergren kinetic rate equation on adsorption reactions. *Scientometrics,* 59, pp. 171–177, DOI: 10.1023/B:SCIE.0000013305.99473.cf.

Ho, Y.S. (2006) Second-order kinetic model for the sorption of cadmium onto tree fern: A comparison of linear and non-linear methods, *Water Research,* 40, pp. 119–125. DOI: 10.1016/j.watres.2005.10.040.

Ho, Y.S., Porter, J.F. & McKay, G. (2002). Equilibrium isotherm studies for the sorption of divalent metal ions onto peat: copper, nickel and lead single component systems, *Water, Air, & Soil Pollution,* 141, pp. 1–33, DOI: 10.1023/A:1021304828010.

Jiao, F., Wijaya, N., Zhang, L., Ninomiya, Y. & Hocking, R. (2011). Synchrotron-Based XANES Speciation of Chromium in the Oxy-Fuel Fly Ash Collected from Lab-Scale Drop-Tube Furnace, *Environmental Science & Technology,* 45, pp. 6640–6646, DOI: 10.1021/es200545e.

Ghanbari Pakdehi, S. & Alipour, M. (2013). Adsorption of Cr(III) and Mg(II) from Hydrogen Peroxide Aqueous Solution by Amberlite IR-120 Synthetic Resin, *Iranian Journal of Chemistry and Chemical Engineering,* 32, pp. 49–55. www.SID.ir.

Liu, X. & Zhang, L. (2015) Removal of phosphate anions using the modified chitosan beads: Adsorption kinetic, isotherm and mechanism studies, *Powder Technology*, 277, pp. 112–119, DOI: 10.1016/j.powtec.2015.02.055.

Luo J, Shen H., Markström, H., Wang, Z. & Niu, Q. (2011). Removal of Cu^{2+} from Aqueous Solution using Fly Ash. *Journal of Minerals and Materials Characterization and Engenering,* 10, pp. 561–571, DOI: 10.4236/jmmce.2011.106043.

Medellin-Castillo, N.A., Padilla-Ortega, E., Regules-Martínez, M.C., Leyva-Ramos, R., Ocampo-Perez, R. & Carranza-Alvarez, C. (2017). Single and competitive adsorption of Cd(II) and Pb(II) ions from aqueous solutions onto industrial chili seeds (Capsicum annuum) waste, *Sustainable Environment Research,* 27, pp. 61–69, DOI: 10.1016/j.serj.2017.01.004.

Mozgawa, W., Jastrzębski, W. & Handke, M. (2006). Cation-terminated structural clusters as a model for the interpretation of zeolite vibrational spectra, *Journal of Molecular Structure,* 792–793, pp. 163–169, DOI: 10.1016/j.molstruc.2005.12.056.

Noroozi, B. & Sorial, G.A. (2013). Applicable models for multi--component adsorption of dyes: A review, *Journal of Environmental Sciences,* 25, 419–429, DOI: 10.1016/S1001-0742(12)60194-6.

Padilla-Ortega, E., Leyva-Ramos, R. & Flores-Cano, J.V. (2013). Binary adsorption of heavy metals from aqueous solution onto natural clays, *Chemical Engineering Journal*, 225, pp. 535–546, DOI: 10.1016/j.cej.2013.04.011.

Polowczyk, I., Ulatowska, J., Koźlecki, T., Bastrzyk, A. & Sawiński, W. (2013). Studies on removal of boron from aqueous solution by fly ash agglomerates, *Desalination,* 310, pp. 93–101, DOI: 10.1016/j.desal.2012.09.033.

Ruhl, L., Vengosh, A., Dwyer, G.S., Hsu-Kim, H. & Deonarine, A. (2010). Environmental Impacts of the Coal Ash Spill in Kingston. Tennessee: An 18-Month Survey, *Environmental Science & Technology*, 44, pp. 9272–9278, DOI: 10.1021/es1026739.

Sarma, G.K., Gupta, S.S. & Bhattacharyya, K.G. (2016). Adsorption of Crystal violet on raw and acid-treated montmorillonite, K10, in aqueous suspension, *Journal of Environmental Management,* 171, pp. 1–10, DOI: 10.1016/j.jenvman.2016.01.038.

Sočo, E. & Kalembkiewicz, J. (2015). Removal of copper(II) and zinc(II) ions from aqueous solution by chemical treatment of coal fly ash, *Croatica Chemica Acta,* 88, pp. 267–279, DOI: 10.5562/cca2646.

Styszko-Grochowiak, K., Gołaś, J., Jankowski, H. & Koziński, S. (2004). Characterization of the coal fly ash for the purpose of improvement of industrial on-line measurement of unburned carbon content, *Fuel,* 83, pp. 1847–1853, DOI:10.1016/j.fuel.2004.03.005.

Szala, B., Bajda, T., Matusik, J., Zięba, K. & Kijak, B. (2015). BTX sorption on Na-P1 organo-zeolite as a process controlled by the amount of adsorbed HDTMA, *Microporous and Mesoporous Materials,* 202, pp. 115–123, DOI: 10.1016/j.micromeso.2014.09.033.

Vieira, R.S., Guibal, E., Silva, E.A. & Beppu, M.M. (2007). Adsorption and desorption of binary mixtures of copper and mercury ions on natural and crosslinked chitosan membranes, *Adsorption*, 13, pp. 603–611, DOI 10.1007/s10450-007-9050-4.

Wang, L. (2012). Application of activated carbon derived from 'waste' bamboo culms for the adsorption of azo disperse dye: Kinetic, equilibrium and thermodynamic studies, *Journal of Environmental Management,* 102, pp. 79–87, DOI: 10.1016/j.jenvman.2012.02.019.

Wieloskładnikowa sorpcja oraz utylizacja odpadu stałego do jednoczesnego usuwania barwnika zasadowego i metalu ciężkiego z układu wodnego

Streszczenie: W pracy przedstawiono prostą modyfikację popiołu lotnego węglowego (FA) za pomocą 30% roztworu H_2O_2 oraz wykorzystanie go jako nowego skutecznego sorbentu do usuwania barwnika organicznego fioletu krystalicznego (CV) w obecności jonów Cu(II) w układzie jedno- i dwuskładnikowym Cu(II)-CV.

Badania FT-IR, TG, SEM-EDS i XRD potwierdziły, że mechanizm sorpcji Cu(II) i CV na FA- H_2O_2 obejmuje proces wymiany jonowej i adsorpcji powierzchniowej.

Porównując wartości zredukowanego testu chi-kwadrat (χ^2/DoF) i współczynnika determinacji R^2 uzyskane dla rozpatrywanych izoterm CV, stopień dopasowania odpowiednich modeli odpowiada następującej kolejności: Jovanović > Langmuir > Elovich > Freundlich > Redlich-Peterson (RP) > Tóth > Halsey > BET. Sorpcja jonów Cu(II) w układzie jednosładnikowym za pomocą FA-H_2O_2 została dobrze opisana za pomocą modelu Langmuira i R-P. Przeanalizowano badania równowagi w układzie dwuskładnikowym wykorzystując rozszerzony model Langmuira (EL), rozszerzony Langmuira-Freundlicha (ELF) i Jain-Snoeyinka (JS).

Estymacja parametrów izoterm sorpcji w układzie binarnym Cu(II)-CV wykazała, że najlepsze dopasowanie wartości obliczonych do danych doświadczalnych dla obu sorbatów posiada model EL oraz model JS, ale tylko w przypadku barwnika CV. Kinetykę sorpcji Cu(II) i CV na FA-H_2O_2 przeanalizowano za pomocą modeli PFO, PSO i dyfuzji wewnątrzziarnowej.